PSFC/JA-20-84

Response of CR-39 nuclear track detectors to protons with non-normal incidence

R. Przybocki, M. Gatu Johnson, G. Sutcliffe, B. Lahmann, F. H. Seguin, J. Frenje, P. Adrian, T. M. Johnson, J. Pearcy, N. V. Kabadi, A. Birkel, R. D. Petrasso

September 2020

Plasma Science and Fusion Center
Massachusetts Institute of Technology
Cambridge MA 02139 USA

This material is based upon the work supported by the Department of Energy, National Nuclear Security Administration under Award No. DE-NA0003868 and by Sandia National Laboratories, Contract No. 2080471.

Submitted to *Review of Scientific Instruments*

Response of CR-39 nuclear track detectors to protons with non-normal incidence

R. Przybocki[a], M. Gatu Johnson, G. Sutcliffe, B. Lahmann, F. H. Seguin, J. Frenje, P. Adrian, T. M. Johnson, J. Pearcy, N. V. Kabadi, A. Birkel, and R. D. Petrasso

Massachusetts Institute of Technology, Cambridge, Massachusetts 02139, USA

Abstract

This paper presents data from experiments with protons at non-normal incidence to CR-39 nuclear track detectors, analyzing properties of detection efficiency, proton track diameter, track contrast, and track eccentricity. Understanding the CR-39 response to protons incident at an angle is important for designing charged particle detectors for inertial confinement fusion (ICF) applications. This study considers protons with incident energies less than 3 MeV. In this regime, an incident angle of 10 degrees has no effect on CR-39 detection efficiency, and >85% detection efficiency is preserved up through 25 degrees in the range of 1.0 to 2.1 MeV. For ICF applications, incident angles above 30 degrees are deemed impractical for detector design due to significant drops in proton detection at all energies. We observe significant reductions in detection efficiency compared to theoretical predictions, particularly at low energies where proton tracks are etched away. Proton track diameter measured by the scan system is observed to decrease with higher incident angles. The track diameters are analyzed with two fitting models, and it is shown that the diameter-energy relation can be fit with existing models at angles up to 30 degrees. Optical contrast of the tracks tends to increase with angle, meaning tracks are fainter, and a larger increase is observed for higher energies. Eccentricity, a measure of how elongated proton tracks are, increases with incident angle and drops after the critical angle. The lowest energy tracks remain nearly circular even at higher angles.

[a] ryanprzybocki@alum.mit.edu

I. Introduction

Solid state nuclear track detectors made from CR-39 plastic are used at Inertial Confinement Fusion (ICF) facilities such as Omega[1] Z[2], and the National Ignition Facility (NIF)[3,4,5]. At these facilities, detector insensitivity to background radiation such as X-rays and electromagnetic noise is paramount, so the detection through mechanical means such as CR-39 is preferred as it avoids the background problems associated with electromagnetic detectors.

When an energetic charged particle collides with CR-39, it damages molecular chains leaving behind a characteristic track. The tracks are revealed through chemical etching with NaOH, which removes material on the surface of the detector as well as inside the tracks. The rate at which tracks are etched ("track etch velocity") is faster than the rate at which the rest of the plastic is etched ("bulk etch velocity"), so the tracks are visible after etching as more track material is removed than surrounding material. These tracks in the plastic vary in diameter and depth, in relation to the rate at which the incident particles lose energy, dE/dx. Detailed discussions of the physics behind proton registration in CR-39 and the associated chemical etching process are given by Hermsdorf[6] and Dörschel et al[7].

The detection efficiency of CR-39 is defined as the ratio of the number of incident particles experimentally detected by the CR-39 to the number expected. Seguin et al. give a CR-39 proton detection efficiency of 100% for incident energies between about 0.5 MeV and 6 MeV[5]. However, these observations for detection efficiency were made for protons at normal incidence to the CR-39, while the response to protons in this energy range incident at an angle has not been well characterized. Also uncertain is how non-normal incidence affects other properties of CR-39 tracks, such as diameter, optical contrast, and track roundness. Certain simplifications to the analysis of normally incident particles are not possible when the particles are incident at an angle, such as automatically filtering out non-circular tracks that usually only appear as background noise.

Previously, Stafford et al. examined the non-normal detection efficiency for protons incident between 3 and 10 MeV, using a single CR-39 etch time of 16 hours[8]. Frenje et al. also simulated the CR-39 response

to non-normal incidence of recoil protons from neutron collisions[9]. As an example of an application where a better understanding of CR-39 response under angled incidence is important, we consider D-D neutron spectrometer designs proposed by B. Lahmann[10]. Both designs involve incident neutrons passing through a conversion foil, colliding elastically with ions and scattering protons at an angle. These recoil protons reach a CR-39 detector at a non-normal incident angle, so characterizing the CR-39 response to non-normal incidence protons is essential for inferring neutron spectra in such a device.

In this paper, we present results from a study where CR-39 is exposed to protons up to 3 MeV while systematically varying the angle of incidence in increments from 0 to 50 degrees. Detection efficiency as well as track characteristics (diameter, contrast, roundness) as a function of angle are discussed. The paper is organized as follows. In Sec. II, the experiment setup is described. In Sec. III, the analysis methods for detection efficiency are explained. In Sec. IV, results are discussed, focusing in turn on efficiency, track diameter as a function of energy, contrast, and eccentricity. Finally, Sec. V concludes the paper.

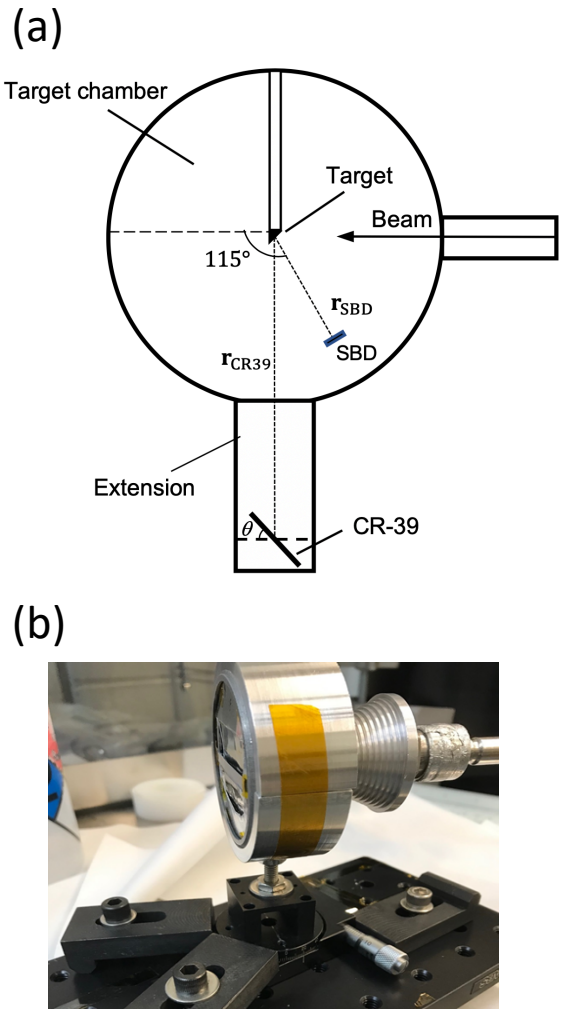

Fig. 1: Setup of the experiment. Fig. 1(a) is a top view of the accelerator chamber, showing the beam line, the target, and the positions of the SBD and CR-39 detector. Fig 1(b) shows the rotating CR-39 enclosure mounted on the pedestal that is placed in the extension chamber.

II. Experiment Design

The experiments in this paper were carried out at the Massachusetts Institute of Technology (MIT) in the Linear Electrostatic Ion Accelerator (LEIA), a facility that develops diagnostics for Omega, Z, and the NIF[11]. In our experiments, a high voltage (125 kV) accelerates deuterium ions down the beam line and onto an Erbium-Deuteride (ErD_2) target in order to produce D-D fusion products. Ports extending off the target chamber allow the placement of CR-39 detectors for experiments. The target chamber, extension ports, and CR-39 holder are shown in Fig. 1.

The branch of the D-D fusion reaction of interest is the following:

$$D + D \rightarrow T^* \, [1.01 \text{ MeV}] + p^* \, [3.02 \text{ MeV}] \quad (1)$$

This reaction branch yields a proton with an energy of 3.02 MeV. We can study energy values at or below this value by introducing range filters that reduce the kinetic energy of these protons. We choose a simple step range filter (SRF) design, which implements fixed aluminum foil thicknesses to downshift the protons to energies below 3 MeV on CR-39. We refer to these aluminum foil arrangements as "filters." To limit the number of independent trials we need, the filter arrangement includes 6 individual aluminum filters overtop one 5 cm diameter piece of CR-39. A schematic for the filter design is shown in Fig. 2.

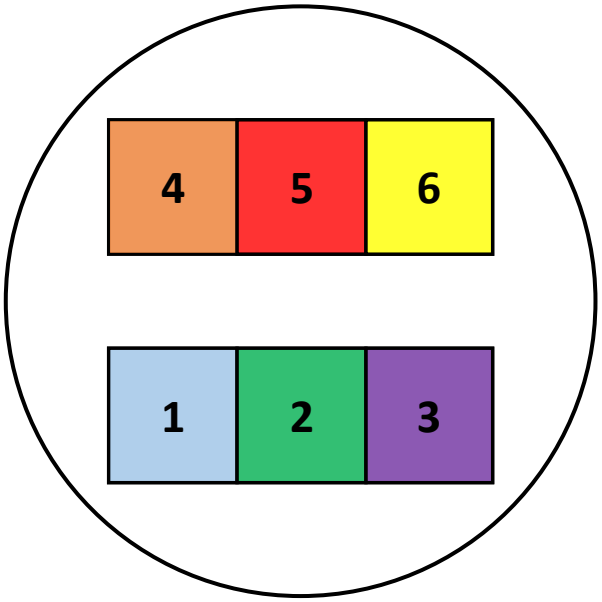

Fig. 2: Schematic for filter arrangement that includes 6 different aluminum thicknesses. Filters are numbered 1 through 6 in order of increasing thickness. Filter thicknesses are shown in Table I.

The post-filter energies were calibrated with a Silicon Surface Barrier Detector (SBD) in the LEIA target chamber. The mean energy measured behind each filter is given in Table I. As shown in the table, the measured spectra had nonzero standard deviations σ, so the incident protons were not perfectly monoenergetic.

Table I: Filter numbers and their corresponding calibrated mean energies, energy distribution widths and aluminum thickness as calculated by SRIM.

Filter	Mean Energy (MeV)	σ (MeV)	Al Thickness (μm)
1	2.898	0.056	5.36
2	2.471	0.069	22.87
3	2.063	0.086	37.72
4	1.668	0.103	50.29
5	1.201	0.127	62.75
6	0.740	0.141	72.35

A consistent experimental procedure is followed for all trials on CR-39, while only varying the angle offset of the CR-39. The filters are aligned with the rows (1–3) and (4–6) parallel to the base of the holding apparatus, and the CR-39 piece is held in place directly behind the filters. The platform holding the CR-39 is placed on tracks within the accelerator's extension that enables a consistent setup at the same distance each time. The accelerator is operated with a deuterium ion beam to produce 3.02 MeV protons as in Eq. (1). Experiments were performed at the following angles (in degrees): 0, 10, 20, 25, 30, 35, 40, 45, 50.

The CR-39 rounds are etched with 6 normal NaOH at 80ºC for fixed durations of 2, 4, and 5 hours then scanned with an optical microscope. Example microscope frames of CR-39 are shown in Fig. 3. A computer program tabulates CR-39 track properties from each experiment, including track density, diameter, contrast, and eccentricity. Proton track density (tracks/cm^2) is used to determine proton flux on the CR-39. Contrast is defined in this experiment as (100% - optical contrast in %), i.e. the darkest proton tracks have the lowest contrast and vice versa. Eccentricity is a measure of the roundness of the tracks, with a higher value denoting a more oblique track.

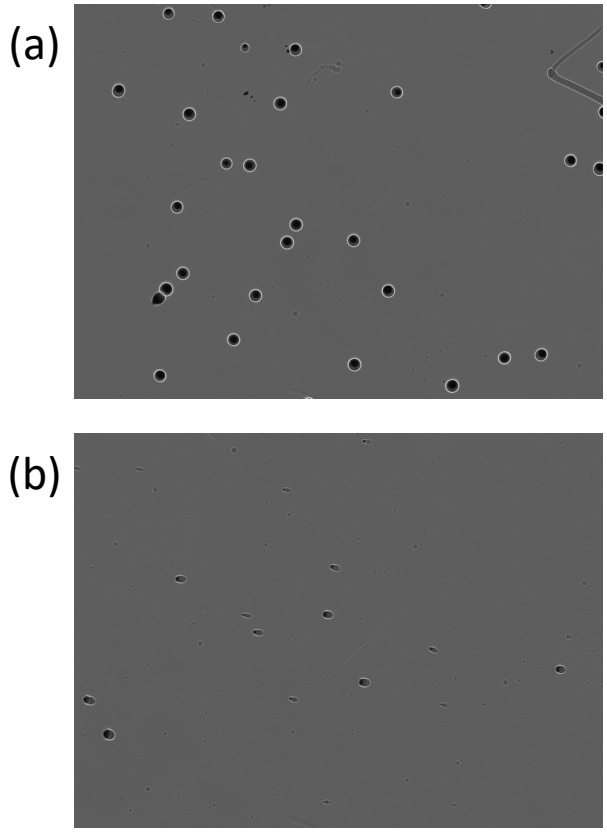

Fig. 3: Sample microscope images of CR-39 behind Filter 3. Fig. 3(a) shows proton tracks at normal incidence, while Fig. 3(b) shows tracks of protons incident at 30 degrees, where the oblique shape of the tracks is visible. Both CR-39 pieces were etched for 2 hours.

III. Analysis methods for detection efficiency

A method is devised to compare the proton flux (tracks/cm^2) across different CR-39 arrangements. To normalize these to a common baseline, we use the observed proton flux on the CR-39 and divide by the theoretical expected flux, which is determined from the SBD flux, adjusted for the different distances and orientations of the SBD and CR-39 detectors. This number is the fraction detection in CR-39 relative to the SBD, which we call the detection efficiency. The SBD is expected to have a 100% detection efficiency for all proton energies of interest. This experiment aims for approximately 20 proton tracks in CR39 per microscope frame to reflect expected conditions in the proposed neutron spectrometers. This corresponds to roughly 16700 tracks per cm^2 in CR39 given a microscope frame area of 0.12 mm^2.

The theoretical expected flux is related to the SBD flux by the inverse square law. We also consider that the angle offset θ of CR-39 reduces its cross-sectional area available for incident protons by a factor of $\cos(\theta)$. Finally, we include a correction factor to account for the different angular positions of the SBD detector and the CR-39. In data from accelerator facility characterization collected previously, the flux measured by an SBD at an angle of 115 degrees (relative to the beam line) is 0.9676 times that of an SBD at 90 degrees (the position of the CR-39 in this experiment)[11]. Combining these contributions, we obtain the following relationship between expected CR-39 flux (tracks/cm^2) and observed SBD counts:

$$\Phi_{\text{expected}} = \frac{C_{\text{SBD}}}{A_{\text{SBD}}} \cdot \left(\frac{r_{SBD}}{r_{CR39}}\right)^2 \cdot \cos(\theta) \cdot \frac{1}{0.9676} \quad (2)$$

Where C_{SBD} is the number of counts observed on the SBD, A_{SBD} is the SBD aperture area (0.172 cm^2 in our experiment), and r_{SBD} and r_{CR39} are the distances from the target to the SBD and CR-39, respectively.

The main contribution to error in our expected flux comes from the uncertainty in the two distance measurements, r_{SBD} and r_{CR39}. These were measured as r_{SBD} = 177.2 ± 2 mm and r_{CR39} = 628 ± 5 mm, making the error on the flux measurement 4%. This provides a lower bound for error bars when comparing measured flux to expected flux for detection efficiency.

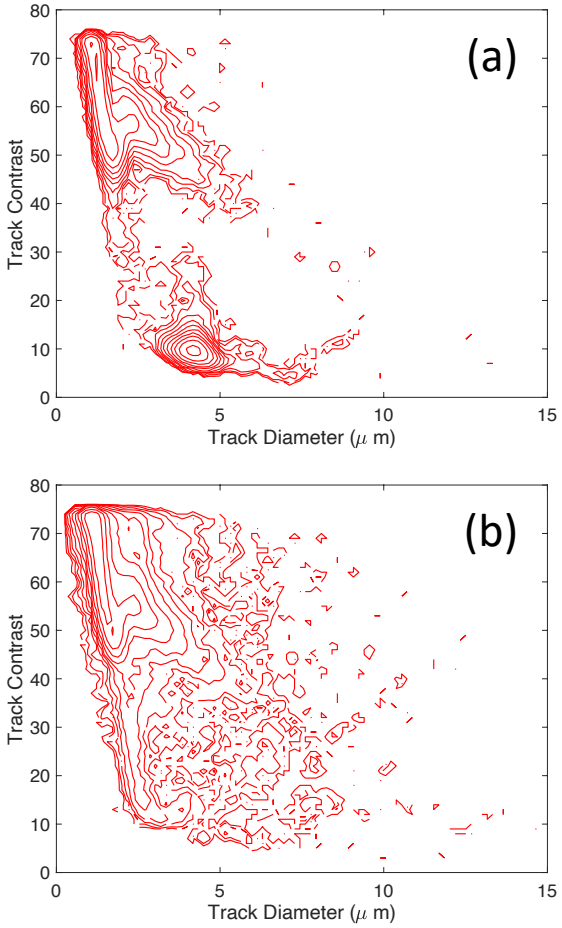

Fig. 4: Example contour plots of track contrast vs. diameter for a section of CR-39. In Fig. 4(a), note the well-defined contour peak at about 4 μm on the top plot. This represents the signal, which is easily separable from the higher contrast background noise. Compare with Fig. 4(b), where the signal begins to blend with noise at higher contrasts.

Tritons, which are also produced in the D-D reaction as shown in Eq. (1), do not interfere with the proton measurements presented here. Tritons are stopped by all filters except the thinnest (filter 1) in our experiment. By placing suitable bounds on the track diameters, the proton tracks are isolated from the triton products for filter 1. For CR-39 arrangements that yield a significant number of high contrast (lighter colored) tracks, additional sources of error must be considered, specifically the large number of intrinsic background tracks that obfuscate the data. Typically, for reasonably low contrast groupings, the proton signal tracks are concentrated at reasonably low contrast and are distinct from high contrast background noise. However, in cases where the proton tracks are high in contrast, they cannot be isolated from the

background noise on the CR-39. A cutoff of contrast ≤ 50% was imposed in our data analysis as resolving signal becomes increasingly difficult above this contrast level. Examples of both high contrast and low contrast cases are shown in Fig. 4. When signal cannot be properly separated from noise there is an additional source of error based on scans of background noise by B. Lahmann[12].

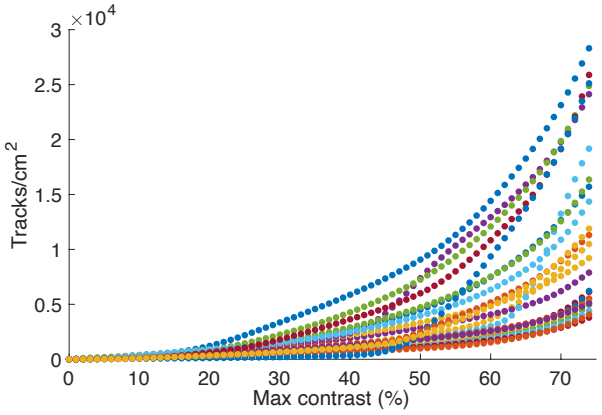

Fig. 5: Level of background noise in tracks/cm^2 at maximum contrast levels up to 75%, across 24 separate CR-39 pieces[12]. Pieces were not exposed to ions prior to processing. Averaging across all pieces at a given contrast yields an uncertainty figure for background tracks.

An uncertainty figure is derived based on the observed error for the number of background tracks, shown across a sample of pieces in Fig. 5. We perform a background subtraction for the CR-39 piece then use the remaining data to find track yield. The fractional uncertainty on this resulting data scales linearly with the background uncertainty, and inversely with the measured number of proton tracks, making the overall fractional error contribution equal to $\beta/\Phi_{\text{measured}}$, where β is the value of background uncertainty.

Summing this background noise uncertainty with the distance measurement uncertainty of 4% in quadrature, we obtain a relative uncertainty on the measured flux in CR-39:

$$\frac{\sigma}{n} = \sqrt{0.04^2 + \left(\frac{\beta}{\Phi_{\text{measured}}}\right)^2} \tag{3}$$

IV. Results

A. Detection Efficiency

An initial overview of the CR-39 scan data reveals an upper limit on angled detection. Above 45 degrees, no proton tracks can be resolved from background noise. We thus consider any offset of ≥45º to be entirely impractical for any detector design.

Detection efficiency data from 0 to 30 degrees with a 2 hour etch is shown in Fig. 6. Additional plots for 4 and 5 hour etch times are shown in Appendix A. For angles through 25 degrees, the detection efficiencies are within error of one another between 1.0 and 2.1 MeV. Moreover, the incident angle of 10 degrees has no effect on detection efficiency for all data above 1.0 MeV, up through the highest energy filter.

Detection efficiency drops at 30 degrees for all incident energies. Above 1.0 MeV, detection at 30 degrees also decreases as energy increases, suggesting that the critical angle at which detection efficiency drops decreases as energy increases.

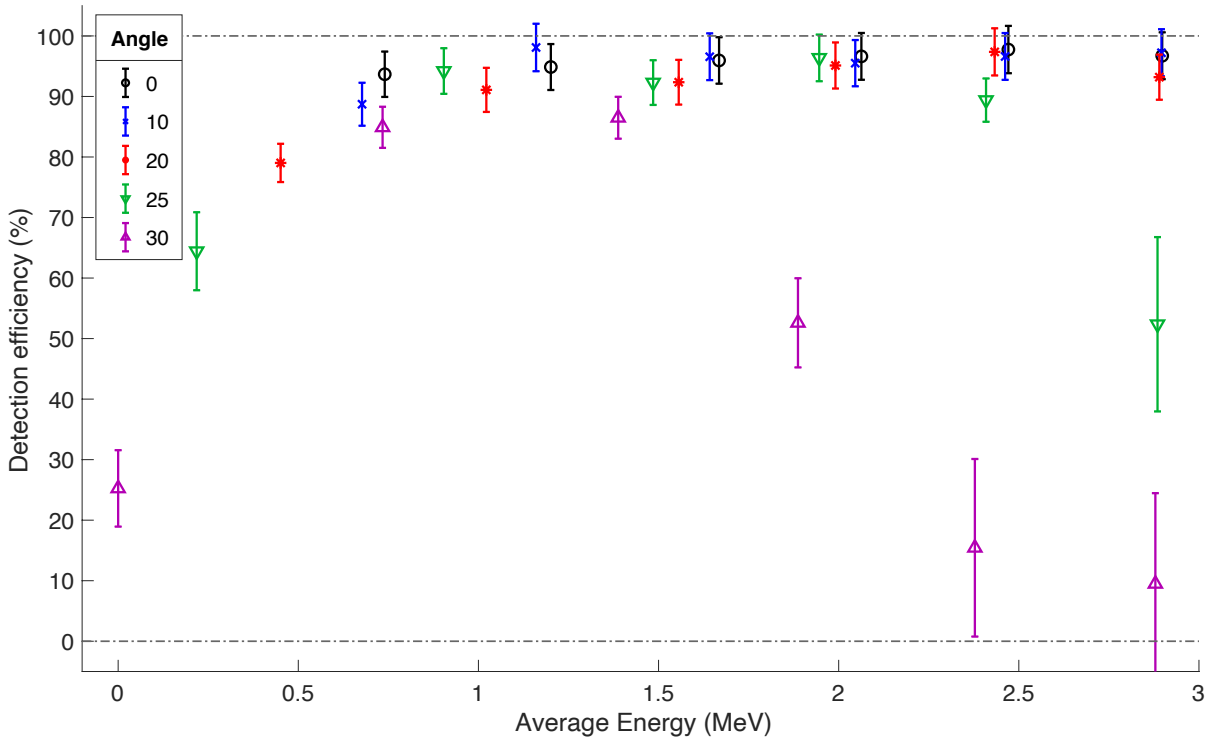

Fig. 6: Detection efficiency of CR-39 for a 2 hour etch procedure vs. incident energy, for incident angles up through 30 degrees.

Theoretical models of track formation in CR-39 define the critical angle as the incident angle at which the perpendicular track etch velocity $\overrightarrow{V_T}$ is equal to the bulk etch velocity $\overrightarrow{V_B}$[8]. Beyond this angle, no tracks are observed.

The track etch and bulk etch velocities in CR-39 can be modeled by the following empirical relation:

$$\left|\overrightarrow{V_T}\right| = \left|\overrightarrow{V_B}\right| \left(1 + k \left(\left[\frac{dE}{dx}(E)\right]_{\frac{keV}{\mu m}}\right)^n\right) \tag{4}$$

Where E is the incident energy of the charged particle and $\frac{dE}{dx}(E)$ the local stopping power in CR-39. Values of k and n are chosen to agree with observed etch behavior[13]: $k = 6 * 10^{-5}$ and $n = 2.76$.

Equating the normal component of $\left|\overrightarrow{V_T}\right|$ with $\left|\overrightarrow{V_B}\right|$ gives us the following expression for the critical angle ψ_c:

$$\cos(\psi_c) = \left(1 + k\left(\left[\frac{dE}{dx}(E)\right]_{\frac{keV}{\mu m}}\right)^n\right)^{-1} \quad (5)$$

In practice, the detection efficiency does not drop immediately from 100% to 0% past the critical angle, due to multiple Coulomb scattering (straggling). The incident energy upon passing through aluminum filters is not a discrete value; rather it is a distribution with non-negligible widths. The standard deviations on the mean energies for the six filters are given in Table I. Thus, we observe a detection dropoff that occurs continuously rather than discretely. Following the approach taken by Stafford et al.[8], we can extrapolate the critical angle in practice as the point of 50% detection efficiency.

We compare the theoretical critical angle to our experiment by plotting the detection efficiency as a function of energy and angle. Plots with three regions of detection efficiency (>85%, 50-85%, <50%) are shown in Fig. 7 along with the theoretical modeled critical angle from Eq. (5).

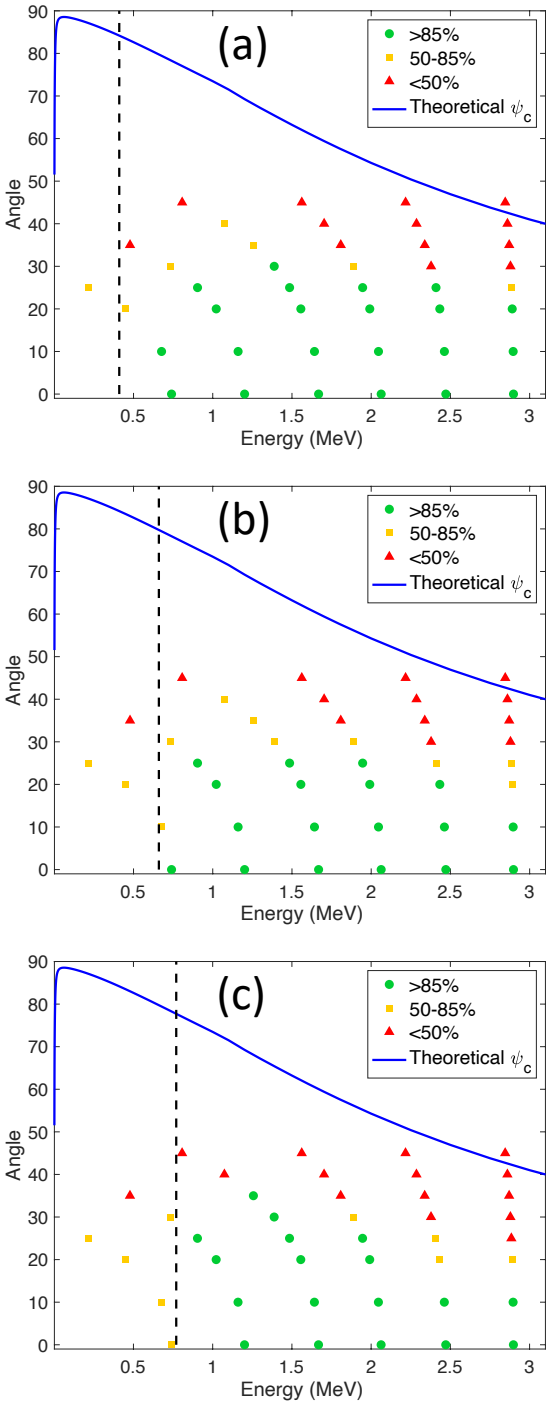

Fig. 7: Observed detection efficiency at 2 hour (a), 4 hour (b), and 5 hour (c) etch times. Detection efficiencies are sorted into three groupings: >85%, 50-85%, and <50%. The solid curve is the theoretical critical angle from Eq. (5). The dashed vertical line represents the energy threshold below which proton tracks would be etched away at the particular etch time.

Experimental data shows more limited regions of detection than suggested by the critical angle theory. The modeled critical angle from Eq. (5) is higher than that observed from the 50% efficiency points. It also

predicts detection at and above 50 degrees for energies below 2.5 MeV. In our experiment, however, we observed no tracks at incident angles greater than 45 degrees.

Moreover, the theory described in Eq. (5) suggests that the critical angle peaks at incident energy of about 0.1 MeV and decreases monotonically with higher energy. However, the maximum critical angle is observed between 1.0 – 1.5 MeV. The critical angle then monotonically decreases beyond 1.5 MeV. We attribute the behavior below 1.0 MeV to low energy protons having a range in CR-39 that is shallower than the etch depth. As explored in calculations by Dörschel et al.[14], in the lower energy limits these proton tracks are etched away and thus not observable. The energy threshold for proton range to exceed etch depth is plotted as a dashed vertical line in Fig. 7 for each etch time and is seen to agree with the efficiency dropoff at low energies. Reflecting this low energy effect, Dörschel et al. models the maximum critical angle to occur at slightly higher energies as etch time increases. These maxima shifts were calculated to be on the order of a few hundred keV. However, the limited energy and angle resolution of our experiment makes this effect difficult to quantify experimentally.

B. Diameter Energy relationship

Proton tracks in CR-39 have a characteristic size that depends on the incident energy and etch times. The relation between track diameter and energy is useful for experiments with step range filters (SRF)[15,16], wedge range filters (WRF)[5,17,18], and the aforementioned neutron spectrometer[10]. Track diameter d is computed by the CR-39 scan system from the track area A by the expression $d = \sqrt{4A/\pi}$.

A plot of the average track diameter vs. incident energy and angle is shown in Fig. 8. We observe that, beyond 1 MeV, the diameter decreases as the incident angle increases. This difference becomes more pronounced as incident energy increases.

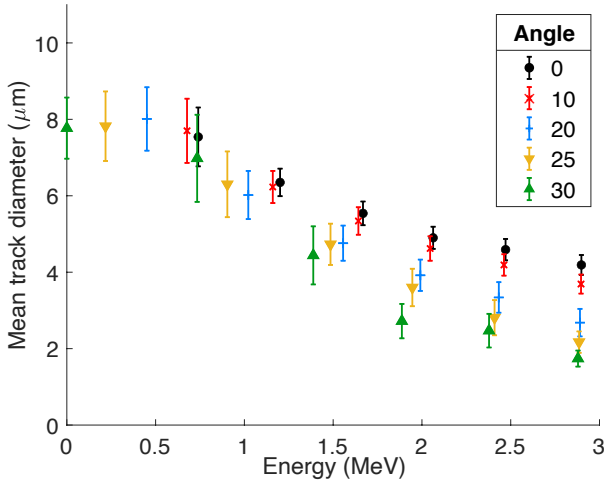

Fig. 8: Track diameter vs. incident energy at 2 hours etch time. From the figure we see that tracks tend to get smaller as the incident angle gets larger. Error bars represent the standard deviation on the track diameter distribution.

Two distinct models have been used to describe the relationship between track diameter and incident energy at normal incidence. Previous work by B. Lahmann[13] modeling tracks etched in CR-39 demonstrated a relationship between track diameter D and incident energy E as follows:

$$D(E) = \frac{2\tau_E|\overrightarrow{V_B}|}{1+k'\left(\frac{E_{MeV}}{Z^2A}\right)^{n'}} \tag{6}$$

Where τ_E is the etch time, k' and n' are the two fit parameters, Z is the charge, and A the atomic mass number. This diameter-energy relationship is dependent on two empirical fit parameters, k' and n', and is thus referred to as the two-parameter model.

A different diameter-energy model typically used for proton data is a larger set of equations that depends on one parameter, c, as well as a measured maximum diameter, D_{max}. This is known as the c-parameter model[13].

Both the two-parameter and c-parameter models have been shown to work equally well for protons at normal incidence to CR-39. However, the use of these fitting models at non-normal incidence has not

previously been tested. Though one would not necessarily expect these models derived for normal incidence to extend to the non-normal cases, we can attempt to fit angled incidence data using these models.

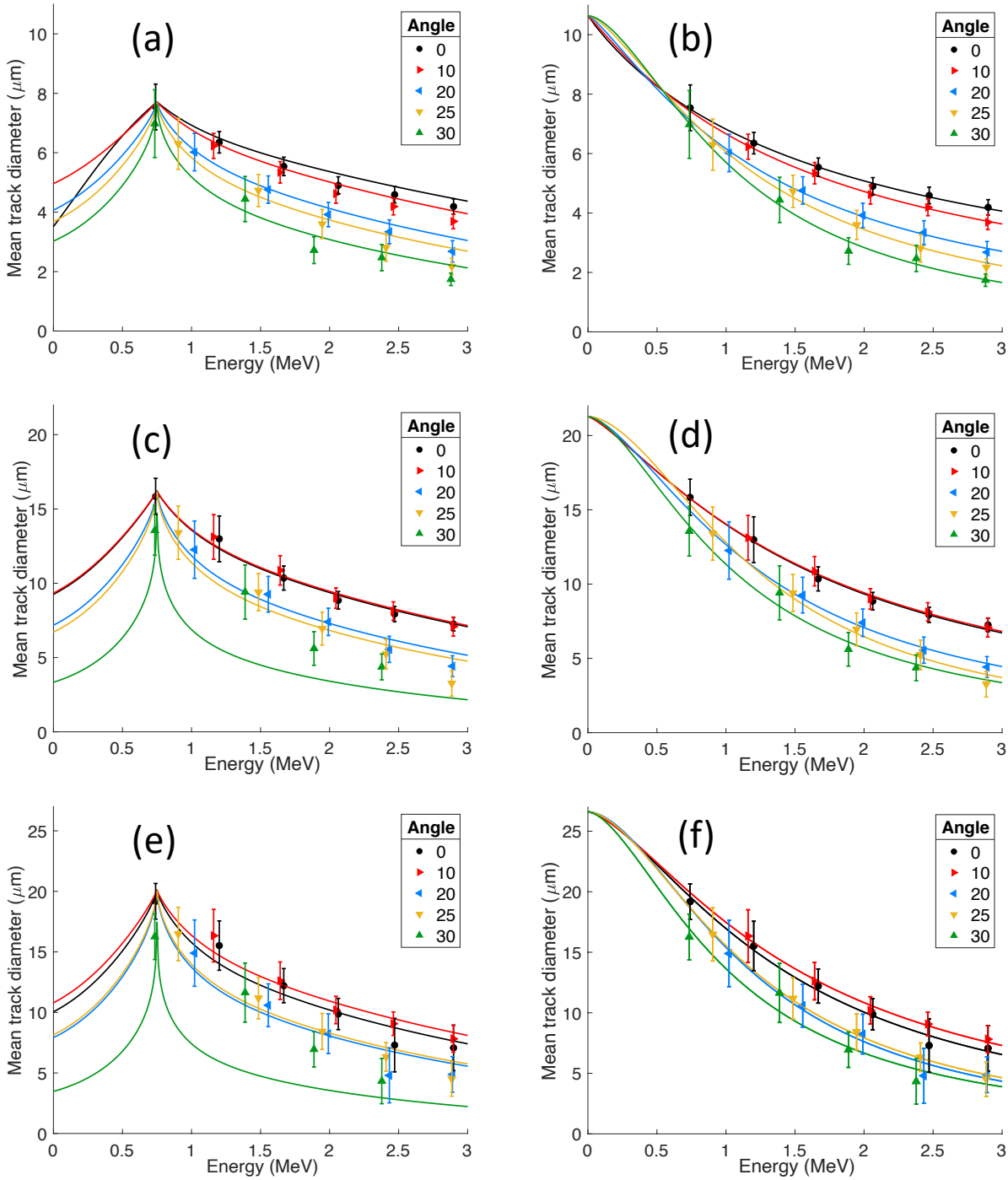

Fig. 9: Comparison of c-parameter and two-parameter fits of track diameter vs. energy for non-normal incident protons. Left column Figs. 9(a), 9(c), and 9(e) are the c-parameter fits for 2-, 4-, and 5-hour etch times, respectively, and the right column Figs. 9(b), 9(d), and 9(f) are two-parameter fits for 2-, 4-, and 5-hour etch times, respectively. As with Fig. 8, error bar size is one standard deviation on the track diameter distribution. Particularly for the 4 and 5 hour etch times, the two-parameter fit describes the data better at non-normal incidence.

The results of the fitting processes are shown in Fig. 9. The track diameter decreases as the incident angle increases. The two-parameter model fits the data noticeably better than the c-parameter model for incident angles ≥ 20 degrees. The c-parameter fit increasingly deviates from the data for greater etch times.

From the diameter-energy fits, it is shown that the two-parameter model can be extended to non-normal incident protons by choosing appropriate fit parameters k' and n'. The c-parameter model with D_{max} reflecting a reasonable experimental maximum diameter does not accurately describe the data at higher angles.

C. Track contrast

Contrast of proton tracks is recorded by the microscope scanning system as a measure of the darkness of the track relative to the average darkness of the frame. A lower contrast indicates a darker track, and vice versa.

A plot of contrast vs. track diameter is shown in Fig. 10. For the 4 highest energy filters, diameter tends to decrease while contrast increases as the incident angle increases. The 2 lowest energy filters exhibit minimal variation in diameter but show an increase in contrast with increasing angle.

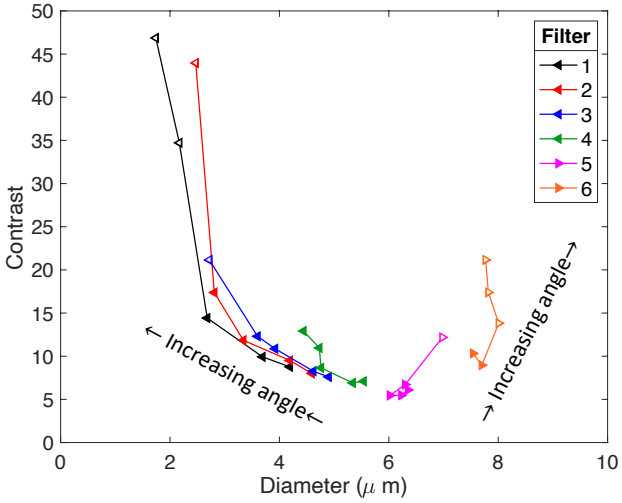

Fig. 10: Proton track contrast vs. track diameter at 2 hour etch time, for each filter. Arrows indicate the direction of increasing angle. Solid data points indicate detection efficiencies >85% at the particular energy and incident angle, while hollow points indicate detection efficiencies below 85%.

The high contrast behavior of filters 1 and 2 at 30 degrees suggests that the loss in detection efficiency (denoted by the hollow marker on the figure) is at least somewhat attributable to the imposed contrast ≤ 50% cutoff. With the mean contrast approaching 50%, it is likely that a significant portion of tracks are lost in the noise above 50% contrast.

D. Track eccentricity

The measure of track roundness is characterized by track eccentricity, which varies from 0 to 100%, with eccentricity 0% being a circular track. A detailed explanation of how eccentricity is computed is given by Seguin et al[5]. In normal incidence experiments, tracks are expected to be nearly circular, so one can ignore tracks above a low eccentricity as background noise. However, in non-normal incidence experiments, we expect a typical track to be elongated, having a nonzero eccentricity. A better understanding of the eccentricity as a function of incidence angle is relevant for data processing of angled incidence applications.

The mean track eccentricity as a function of incidence angle is plotted in Fig. 11. As expected, eccentricity increases with incidence angle. Eccentricity also increases with energy, so the higher energy particles produce more eccentric tracks. At the lowest energy filter, shown in Fig. 11(f), the tracks remain nearly circular for all angles.

Also shown in Fig. 11 is the tendency for tracks to become more rounded beyond the critical angle. This is most pronounced at the higher energies shown in Figs. 11(a) and 11(b). An approximate critical angle is determined from the 50% detection efficiency points at 2, 4, and 5 hours in Fig. 7. The pattern of eccentricity increasing with angle remains up to the critical angle (denoted by the dashed vertical line in the figures), at which point eccentricity drops noticeably. The eccentricity drop correlates with the drop in detection efficiency, so we believe this is an artificial effect arising from limited proton detection. This effect is difficult to probe further due to the lack of reliable data beyond the critical angle, where very few tracks are visible.

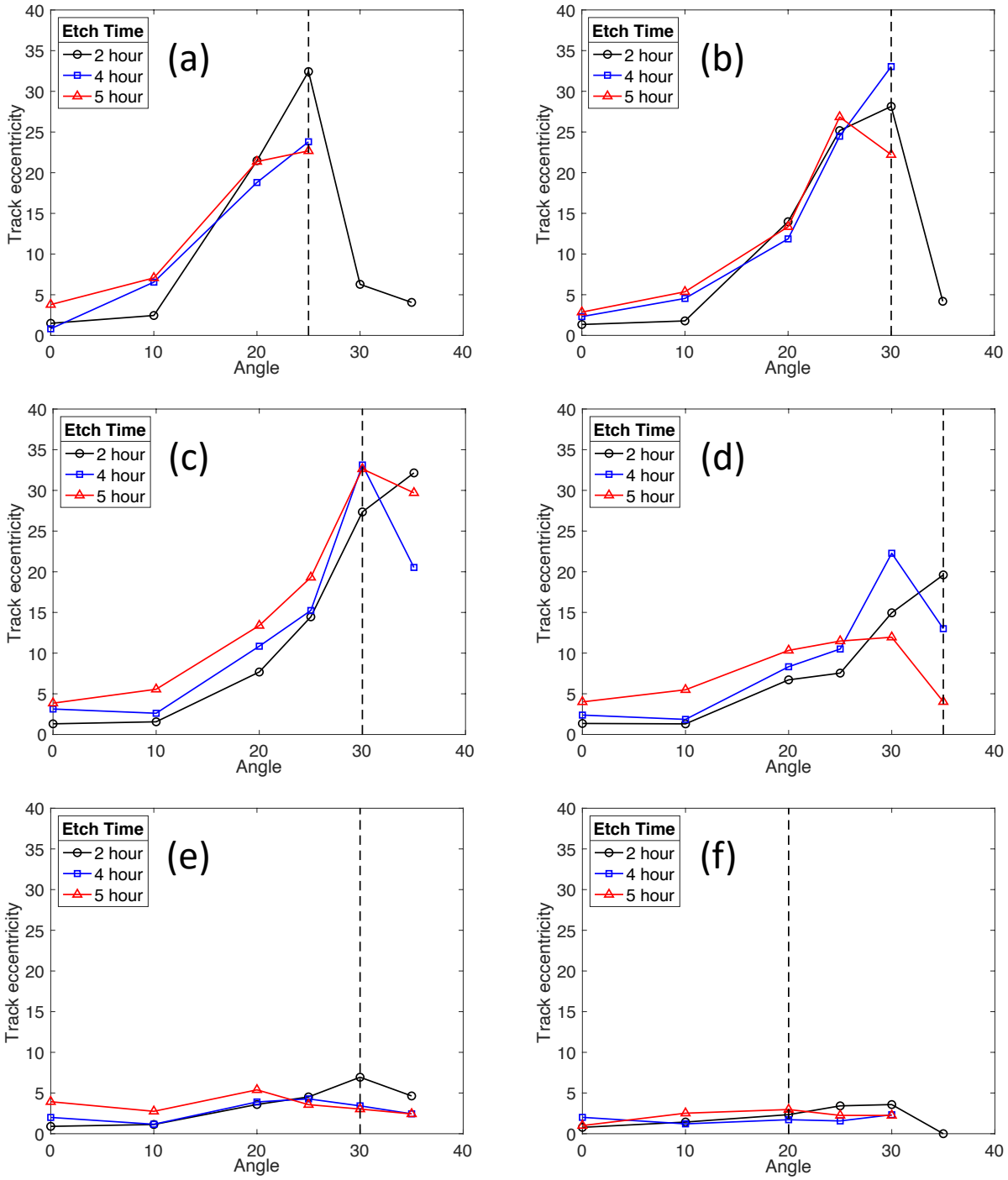

Fig. 11: Track eccentricity data for all filters at 2, 4, and 5 hour etch times. Figs. 11(a)-11(f) plot data from filters 1-6, respectively. The dashed vertical line on each plot represents the extrapolated critical angle from the detection efficiency data.

V. Conclusions

In this paper, we have examined the behavior of the nuclear track detector CR-39 in response to protons incident at an angle. These results are relevant for ICF applications that use CR-39 in configurations with non-normal incident charged particles. As a specific example, this data is essential for a recently proposed neutron spectrometer at the Z facility.

The study of detection efficiency at proton incident angles up to 50 degrees offers a number of insights relevant for spectrometer design. In the energy regime studied (< 3 MeV), angles beyond 45 degrees produce no usable data. In general, incident angles ≥ 30 degrees had detection efficiencies well below 100% and were thus shown to be impractical for detector design. We propose a usable energy range between 1.0 and 2.1 MeV for spectrometers involving proton incident angles up to 25 degrees. This energy range can be extended up to 2.9 MeV for incident angles of 10 degrees or less.

The detection efficiency experiments in this paper yield limitations on critical angle theory. The critical angle observed in the data is significantly lower than that predicted by theory. The region of proton detection is thus far more limited than the critical angle theory predicts. A detection dropoff is also observed at the lowest energies, which is accounted for by predictions for bulk etch depth versus proton range in CR-39. Low energy protons yield shallow tracks that can vanish during the etch process.

The track diameter vs. energy relationship was studied for non-normal incidence protons. We found that the track diameter decreases with increasing incident angle. Two fitting methods for the normal incidence case were discussed; the two-parameter model was shown to extend to angles above 20 degrees, while the c-parameter model did not fit the data.

Contrast, a measure of track darkness, was studied in its relation to track diameter and energy. Contrast tends to increase with angle, while the track diameter decreases. These effects are more

pronounced for higher energies. At the two highest energies, the average contrast near 50% is proposed as a possible mechanism for the reduced detection efficiency at 30 degrees incidence.

The track eccentricity, measuring roundness of the proton tracks, was found to increase as the incident angle increases. The rate of increase is greatest for higher energies, and the lowest energy tracks remain nearly circular.

Acknowledgements

The authors sincerely thank Bob Frankel and Ernie Doeg for help with CR-39 processing. This material is based upon the work supported by the Department of Energy, National Nuclear Security Administration under Award No. DE-NA0003868 and by Sandia National Laboratories, Contract No. 2080471. This report was prepared as an account of work sponsored by an agency of the United States Government. Neither the United States Government nor any agency thereof, nor any of their employees, makes any warranty, express or implied, or assumes any legal liability or responsibility for the accuracy, completeness, or usefulness of any information, apparatus, product, or process disclosed, or represents that its use would not infringe privately owned rights. Reference herein to any specific commercial product, process, or service by trade name, trademark, manufacturer, or otherwise does not necessarily constitute or imply its endorsement, recommendation, or favoring by the United States Government or any agency thereof. The views and opinions of authors expressed herein do not necessarily state or reflect those of the United States Government or any agency thereof.

Appendix A: Detection Efficiency plots

Similar plots to Fig. 6 were made for the 4 and 5 hour etch times, shown in Fig. 12. In comparison to the 2 hour etch time plot, these plots illustrate the detection dropoff at low energies for higher etch times, which we have attributed to the shallow tracks being etched away.

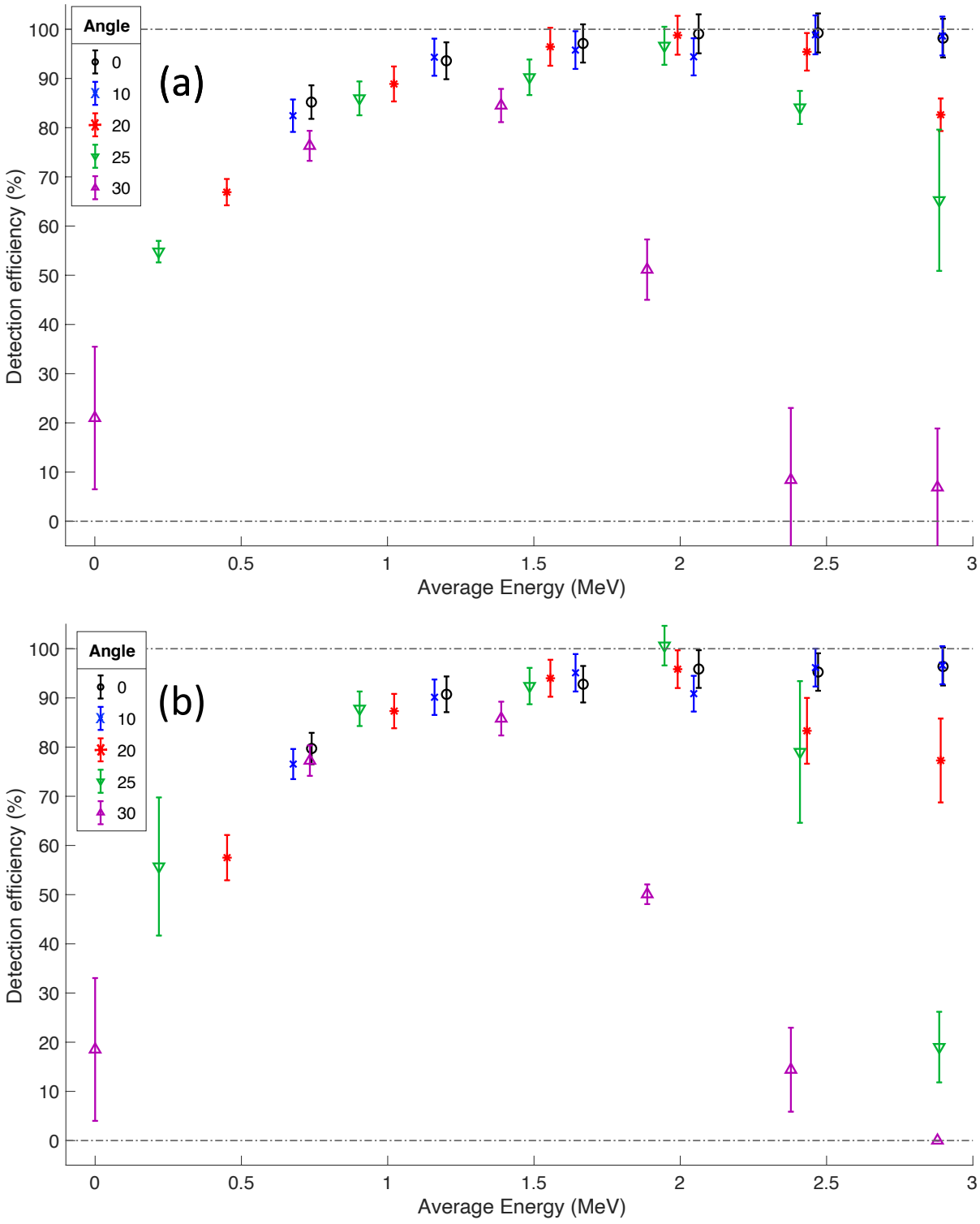

Fig. 12: Detection efficiency vs. energy for 4 and 5 hour etch times, in Figs. 12(a) and 12(b), respectively. The dropoff in detection at low energies due to tracks etched away is visible here in comparison to the two hour etch time.

Appendix B: Contrast vs. Incident Angle

The track contrast data is plotted in Fig. 13, in the same manner as the eccentricity data from Fig. 11. The contrast tends to increase with angle, with the rate of increase decreasing as incident energy decreases. At the two lowest energies, the higher etch time (5 hours) has a higher contrast. This can be attributed to tracks becoming lighter as they are nearly etched away at higher etch times.

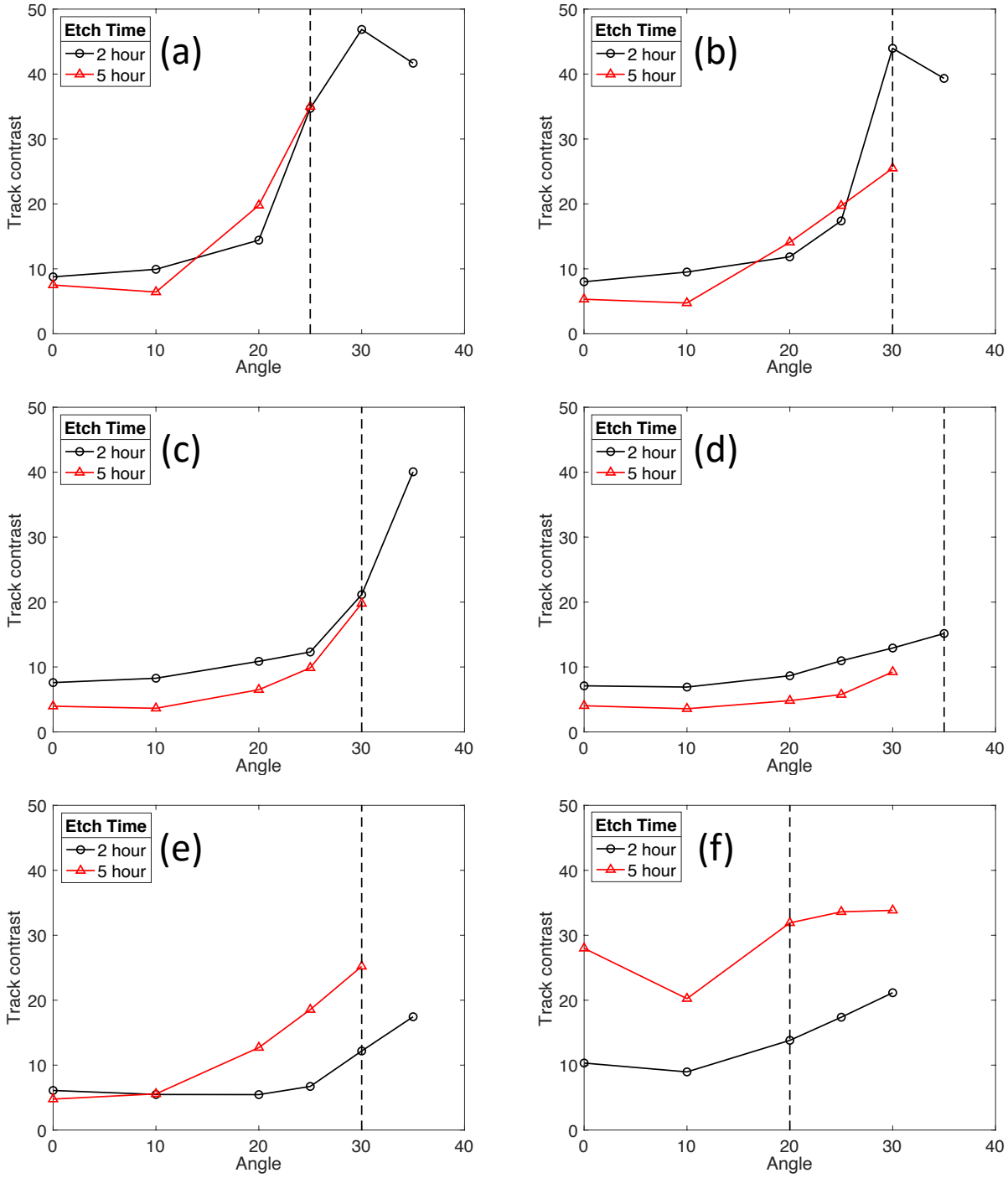

Fig. 13: Plots of track contrast vs. incident angle for 2 and 5 hour etch times. Figs. 13(a)-13(f) plot data from filters 1-6, respectively. The dashed vertical line is the extrapolated critical angle for each filter. Contrast (how light the track is) tends to increase with angle, which is more pronounced at the highest energy filters 13(a) and 13(b).

Data Availability

The data that support the findings of this study are available from the corresponding author upon reasonable request.

References

[1] T. R. Boehly, D. L. Brown, R. S. Craxton, R. L. Keck, J. P. Knauer, J. H. Kelly, T. J. Kessler, S. A. Kumpan, S. J. Loucks, S. A. Letzring, F. J. Marshall, R. L. McCrory, S. F. B. Morse, W. Seka, J. M. Soures, C. P. Verdon. Opt. Commun. **133**, 495 (1997).

[2] M. Cuneo, M. C. Herrmann, D. B. Sinars, S. A. Slutz, W. A. Stygar, R. A. Vesey, A. B. Sefkow, G. A. Rochau, G. A. Chandler, J. E. Bailey, J. L. Porter, R. D. McBride, D. C. Rovang, M. G. Mazarakis, E. P. Yu, D. C. Lamppa and K. J. Peterson, IEEE Transactions on Plasma Science **40**, no. 12, 3222 (2012).

[3] G. H. Miller, E. I. Moses and C. R. Wuest, Nucl. Fusion **44**, S228 (2004).

[4] S. A. Durrani and R. K. Bull, Solid State Nuclear Track Detections, Principles, Methods and Applications, New York: Pergamon, 1987.

[5] F. H. Seguin, J. A. Frenje, C. K. Li, D. G. Hicks, S. Kurebayashi, J. R. Rygg, B. E. Schwartz, R. D. Petrasso, S. Roberts, J. M. Soures, D. D. Meyerhofer, T. C. Sangster, J. P. Knauer, C. Sorce, V. Yu, C. Stoeckl, T. W. Phillips, R. J. Leeper, K. Fletcher and S. Padalino, Rev. Sci. Instrum. **74**, 975 (2003).

[6] D. Hermsdorf, Radiat. Meas. **46**, 396 (2011).

[7] B. Dörschel, D. Fülle, H. Hartmann, D. Hermsdorf, K. Kadner, and Ch. Radlach, Radiat. Prot. Dosim. **71**, no. 2, 99 (1997).

[8] P. M. Stafford, J. L. Horton, K. R. Hogstrom, P. M. DeLuca, Jr., and D. Holslin, Nucl. Tracks Radiat. Meas. **14**, 373 (1988).

[9] J. A. Frenje, C. K. Li, F. H. Seguin, D. G. Hicks, S. Kurebayashi, R. D. Petrasso, S. Roberts, V. Yu, D. Glebov, D. Meyerhofer, T. C. Sangster, J. M. Soures, C. Stoeckl, C. Chiritescu, G. J. Schmid and R. A. Lerche, Rev. Sci. Instrum. **73**, 2597 (2002).

[10] B. Lahmann, M. Gatu Johnson, K. D. Hahn, J. A. Frenje, D. J. Ampleford, B. Jones, M. A. Mangan, A. Maurer, C. L. Ruiz, F. H. Seguin, and R. D. Petrasso, Rev. Sci. Instrum. **91**, 073501 (2020)

[11] N. Sinenian, M. J. E. Manuel, A. B. Zylstra, M. Rosenberg, C. J. Waugh, H. G. Rinderknecht, D. T. Casey, H. Sio, J. K. Ruszczynski, L. Zhou, M. Gatu Johnson, J. A. Frenje, F. H. Seguin, C. K. Li, R. D. Petrasso, C. L. Ruiz and R. J. Leeper, Rev. Sci. Instrum. **83**, 043502 (2012).

[12] B. Lahmann, "Background noise on CR-39 track detectors" (unpublished).

[13] B. Lahmann, M. Gatu Johnson, J. A. Frenje, Y. Yu Glebov, H. G. Rinderknecht, F. H. Seguin, G. Sutcliffe, and R. D. Petrasso, Rev. Sci. Instrum. **91**, 053502 (2020).

[14] B. Dörschel, D. Fülle, H. Hartmann, D. Hermsdorf, K. Kadner and Ch. Radlach, Radiat. Prot. Dosim. **71**, no. 4, 245 (1997).

[15] B. Lahmann, M. Gatu Johnson, J. A. Frenje, A. J. Birkel, P. J. Adrian, N. Kabadi, J. H. Kunimune, T. M. Johnson, J. A. Pearcy, B. L. Reichelt, F. H. Seguin, G. Sutcliffe, and R. D. Petrasso, "Extension of charged-particle spectrometer capabilities for diagnosing implosions on OMEGA, Z, and the NIF", (submitted to Rev. Sci. Instrum.)

[16] M. J. Rosenberg, A. B. Zylstra, J. A. Frenje, H. G. Rinderknecht, M. Gatu Johnson, C. J. Waugh, F. H. Seguin, H. Sio, N. Sinenian, C. K. Li, R. D. Petrasso, V. Yu. Glebov, M. Hohenberger, C. Stoeckl,

T. C. Sangster, C. G. Yeamans, S. LePape, A. J. Mackinnon, R. M. Bionta, B. Talison, D. T. Casey, O. L. Landen, M. J. Moran, R. A. Zacharias, J. D. Kilkenny, and A. Nikroo, Rev. Sci. Instrum. **85**, 103504 (2014).

[17] F. H. Seguin, N. Sinenian, M. Rosenberg, A. Zylstra, M. J.-E. Manuel, H. Sio, C. Waugh, H. G. Rinderknecht, M. Gatu Johnson, J. Frenje, C. K. Li, R. Petrasso, T. C. Sangster, and S. Roberts, Rev. Sci. Instrum. **83**, 10D908 (2012).

[18] A. B. Zylstra, J. A. Frenje, F. H. Séguin, M. J. Rosenberg, H. G. Rinderknecht, M. Gatu Johnson, D. T. Casey, N. Sinenian, M. J.-E. Manuel, C. J. Waugh, H. W. Sio, C. K. Li, R. D. Petrasso, S. Friedrich, K. Knittel, R. Bionta, M. McKernan, D. Callahan, G. W. Collins, E. Dewald, T. Döppner, M. J. Edwards, S. Glenzer, D. G. Hicks, O. L. Landen, R. London, A. Mackinnon, N. Meezan, R. R. Prasad, J. Ralph, M. Richardson, J. R. Rygg, S. Sepke, S. Weber, R. Zacharias, E. Moses, J. Kilkenny, A. Nikroo, T. C. Sangster, V. Glebov, C. Stoeckl, R. Olson, R. J. Leeper, J. Kline, G. Kyrala, and D. Wilson, Rev. Sci. Instrum. **83**, 10D901 (2012)